TRANSONIC PRESSURE DRAG COEFFICIENT FOR AXISYMMETRIC BODIES

by

O. Biblarz and E. Priyono

Naval Postgraduate School

Monterey, CA 93943-5106, USA

ABSTRACT

This is an investigation of the transonic pressure-drag coefficient over axisymmetric bodies, with a set of unique afterbody contours developed by the authors. The contour surfaces were obtained from an exact solution of the small-perturbation transonic equation. In this work, Computational Fluid Dynamics (CFD) is used to establish the afterbody contour drag. This drag is then compared to that a conical afterbody; subsequently, a complete body composed of an arbitrary forebody (an ellipsoid) and variable afterbody (ours and conical contours) is analyzed. Euler as well as Navier-Stokes flow-solvers were applied to the geometries of interest giving Mach-number mappings for inviscid and viscous flows as well as pressure drag coefficient magnitudes, and depicting shock wave locations. Based of these results, it can be shown that our afterbody contours will decrease by 15% the peak of the pressure drag coefficient (C_d) versus Mach number curves which are evidenced in conical afterbodies in the transonic regime. Our contours can then be used to design low pressure drag surfaces for such shapes as missiles, projectiles and aircraft engine nacelles.

Introduction

Aerodynamic drag represents a significant adverse force on all flying objects such as aircraft, missiles and projectiles. A high drag force reduces the craft's range capability or equivalently requires more energy to achieve a certain range. Any effort to reduce the drag coefficient in the design process must concentrate on reducing the wake and pressure drag (inclusive of wave drag) contributions to the total drag.

Inherent difficulties, coupled with the presence of shocks which cause boundary layer separation, have resulted in the creation of many approximate methods of solution in the design of transonic airfoils and the like[1,2,3].

On the other hand, the use of numerical simulation Computational Fluid Dynamics (CFD) to predict aerodynamic characteristics greatly increases possibilities to improve design optimization at relatively low cost and allows for ease of design changes. Using the latest capabilities of Euler as well as Navier-Stokes flow-solvers, it is possible to compute the flow over axi-symmetric bodies with various contours in the transonic regime[4,5]. These flow solvers, however, are designed to "test" a given configuration having no contour generating capabilities. The shapes of afterbodies is thus restricted to the traditional ogives and cones. This work implements solutions to the small perturbation equation for transonic flow which have been developed at the Naval Postgraduate School. The technique is briefly summarized below.

For axially symmetric flow, where the conditions are the same in every meridian plane, there is no variation with polar angle θ so the small perturbation, non-linear, axi-symmetric transonic potential equation can be written as follows:

$$\frac{\partial^2 \phi}{\partial r^2} + \frac{1}{r}\frac{\partial \phi}{\partial r} + (1-M_\infty^2)\frac{\partial^2 \phi}{\partial x^2} = \frac{M_\infty^2(\gamma+1)}{U}\frac{\partial \phi}{\partial x}\frac{\partial^2 \phi}{\partial x^2} \quad (1)$$

or rewriting in shorthand notation,

$$\phi_{rr} + \frac{1}{r}\phi_r + (1-M_\infty^2)\phi_{xx} = \frac{M_\infty^2(\gamma+1)}{U}\phi_x\phi_{xx} \quad (2)$$

Reference 6 introduces a modified potential equation for axi-symmetric flows

$$\frac{1}{r}\frac{\partial}{\partial r}(r\phi_r) + (1-M_\infty^2)\phi_{xx} = \phi_x\phi_{xx} \quad (3)$$

where the modified velocity potentials are :

$$\phi_x = M_\infty^2(\gamma+1)\frac{u_x}{U}, \qquad \phi_r = M_\infty^2(\gamma+1)\frac{u_r}{U} \qquad (4)$$

Solutions to the modified transonic eq. (3) have been given by Biblarz[6,7] using the separation of variables approach with a potential function $\phi(x,r)$ of the form

$$\phi(x,r) = \xi(x)\eta(r) + (1-M_\infty^2)x \qquad (5)$$

Substituting the above ϕ function in the modified transonic eq. (3) results in two ordinary, second order, non-linear differential equations

$$\frac{d\xi}{dx}\frac{d^2\xi}{dx^2} - \lambda\xi = 0 \qquad (6)$$

and

$$\frac{d^2\eta}{dr^2} + \frac{1}{r}\frac{d\eta}{dr} - \lambda\eta^2 = 0 \qquad (7)$$

where λ is the separation constant.

Equation (6) has been numerically integrated and plotted in the transonic range. A "patching" technique discussed in Ref. 8 has been used here. Equation 7 is solved by a perturbation method[9].

Pressure Coefficient

The linearized pressure coefficient approximation for axi- symmetric flow turns out to be

$$C_p = -\frac{2u_x}{U_\infty} \qquad (8)$$

Recall the modified axial velocity potential, eq. (4), yields

$$C_p = \frac{-2\,\phi_x}{M_\infty^2(\gamma+1)} \qquad (9)$$

Finally, rewriting the pressure coefficient C_p as

$$C_p = \frac{-2}{M_\infty^2(\gamma+1)}\left[0.2208\bar{\eta}\left[\xi^2 + |(1-M_\infty^2)|^{1.7574}\right]^{\frac{1}{3}} + (1-M_\infty^2)\right] \qquad (10)$$

Boundary Surfaces

In terms of perturbation velocities this boundary condition becomes

$$\left(\frac{dr}{dx}\right)_{surface} = \frac{u_r}{U_\infty} \qquad (11)$$

Finally leading to,

$$\int_{\bar{r}_0}^{\bar{r}} \frac{d\bar{r}}{\sqrt{\left[\frac{8}{\bar{r}^3}-2.8284\,|1-M_\infty^2|\,\bar{r}^{1.8284}-0.1512(1-M_\infty^2)^2\bar{r}^{6.657}\right]}} = \frac{-0.0326}{M_\infty^2(\gamma+1)}\int_0^{\bar{x}}\xi\,d\bar{x} \qquad (12)$$

where $\quad \bar{r}_0 = \dfrac{1.2074}{|1-M_\infty^2|^{0.2071}}$.

Al-hashel[8] reports on computations of eq.(12) using numerical integration. Boundary surfaces in dimensional and non-dimensional (normalized) form for $M_\infty = 1.05$, 1.10 and 1.20 are indicated. Based on these calculations, the geometric grid of the afterbody for Mach number 1.10 and 1.20 are developed for further study with CFD.

This work also examines conical afterbodies as a solid afterbody boundary surface with base diameter ratio (d_b/d_m) of 0.50 and 0.75 and conical turning angle (β) of 26.6 and 14.0 degree respectively[10,11]. Then, for further investigation, the complete bodies as a solid boundary surface are generated, with a kind of forebody (ellipsoid) joined with the contour surface afterbodies as well as the conical afterbodies.

Computational Fluid Dynamics

As a model based method, CFD can provide the convenience of being able to switch off specific terms in the governing equations[12], so as to assist the researcher in understanding the contributions of various physical factors.

In this work, CFD was used to compute the axi-symmetric flow over the afterbody geometry of models only (the boundary surfaces obtained by the small perturbation method[8] and conical afterbody) and over complete body models which are composed of forebody (ellipsoid) and the previously mentioned afterbodies.

Grid Generation

The computer programs GRAPE[13] and GRIDGEN2D[14] are tools used to generate two-dimensional structured grids about airfoils and other shapes by the use of algebraic or Poisson differential equation solvers. GRAPE was used for the geometry with smooth contour surfaces, while GRIDGEN2D was used for the geometry with a conical afterbody with non-smooth points. The important characteristics in a grid generation technique are the ability to specify the spacing between mesh points at the boundary, in the direction normal to the boundary, and the control of the angles with which mesh lines intersect the boundaries which is known as orthogonality.

We developed a fine grid for complete bodies, where the radius of outer boundary is set up to be five times of the body's length. Figure (1) is a typical fine grid for the complete body with a conical afterbody and a complete body with contour surface afterbody.

Results

The OVERFLOW program[15] was developed by the NASA Ames Research Center. It uses either 3-D Euler or Navier-Stokes flow-solvers for inviscid/viscous flow, by setting the viscosity input parameter in the input file.

Results of this CFD investigation are grouped into the corresponding geometric shape, namely, afterbody only and complete body. The Euler flow-solver (inviscid flow) was applied to all axi-symmetric bodies, and for the afterbody models, both Euler and Navier-Stokes (viscous flow) were applied. Most of the calculations converged in 500 iterations, meaning that the residual history achieved a two order of magnitude drop.

Results can be analyzed by interpreting the Mach number contours surrounding the body surfaces where one can be determine the characteristics of the flow field. In addition, the drag coefficient C_d, can be obtained as an output from OVERFLOW. Hence, in the sequences of mach number, one can describe the significant flow characteristic of each geometric shape.

Afterbodies

An Euler as well as a Navier-Stokes flow-solver were applied as previously described. The approaching free stream Mach number (ranging from 1.05 to 1.50) starts from the mid-section of the afterbodies, then the flow follows along the afterbody surface until it reaches a maximum local Mach number. The maximum local Mach number for viscous flow is always lower compared to in the inviscid flow. This may be caused by the viscous flow itself since we are taking into account shear forces in the boundary layer.

In inviscid flow, the shocks form right at the surface. The location of the shock depends on the specific afterbody contour and the approaching Mach number; at the higher Mach numbers the shock appears a bit further downstream. As shown in figures (2) and (3), there are differences as a result of viscosity. Figure (3) shows the boundary layer by the increment of Mach number away form the surface. Weak shocks are formed further downstream compared to inviscid flow. Flow separation occurs in the starting contour region and is followed by circulating flow in the base region.

For the conical afterbody, the approaching free stream Mach number increases following the mid-section surface, then an expansion occurs at the turning angle region, until the maximum local Mach number is reached. A weak shock is formed at the end of the boattail region as shown in figure (4), while for the viscous flow, the weak shock develops away from boattail surface due to the boundary layer and the separation of the flow, figure (5). The circulating flow in the base region is more significant than in the inviscid flow as depicted. In addition, for viscous flow, the maximum local Mach number for the conical afterbody is higher than for the contoured afterbody.

For each afterbody, the pressure drag coefficient (C_d) versus free stream Mach number (M_∞) for inviscid and

viscous flow are plotted in figure (6). The negative sign of C_d is due to the fact that the calculation of pressure starts from mid-section through the base of afterbody and ignores the forebody pressure. These results show that, as expected, the pressure drag coefficient is higher for viscous flows than for inviscid flows for each given afterbody. This is caused by the both viscosity and the pressure distribution difference in the flow field. In addition, it can be seen from the chart, that the C_d for the afterbody with small perturbation solution contour Mach 1.10 (SPS1.1) has the lowest C_d values over the entire Mach number range. Therefore, the SPS1.1 contour shows to be relatively the best among these afterbodies.

Complete Bodies

Complete bodies consist of an arbitrary forebody (ellipsoid) joined to various afterbodies such as the small perturbation solution contours (SPS_1.1 and SPS_1.2) and conical afterbodies. The approaching free stream Mach number (M_∞ ranging from 0.50 to 1.50) starts from outer boundary with a of distance 5 times body's length for the fine grid. For this grid, the bow shock dies out before reaches the outer boundary.

The flow stagnates on the nose and then follows the body surface until it reaches a maximum local Mach number as tabulated in Table 1. The critical Mach number for these complete bodies is approximately at $M_\infty = 0.70$, where the maximum local Mach number reaches unity at the shoulder region.

TABLE 1.
MAXIMUM LOCAL MACH # FOR COMPLETE BODY

Mach #	SPS_1.1	SPS_1.2	SPS-26	CONE-14
0.50	0.68	0.66	0.70	0.64
0.75	1.10	1.10	0.95	1.05
0.85	1.30	1.30	1.50	1.30
0.95	1.45	1.45	1.65	1.40
1.05	1.60	1.60	1.75	1.45
1.10	1.70	1.70	1.75	1.50
1.20	1.80	1.80	1.85	1.60
1.30	1.90	1.90	1.90	1.70
1.50	2.10	2.10	2.10	1.90

A supersonic approaching free stream Mach number, is depicted in figure (7) for SPS_1.2. A bow shock should be apparent in front of the nose. A subsonic region is formed between bow shock and the nose, then the flow accelerates along the forebody surface up to a supersonic region in the mid-section. The expansion flow occurs in the starting contour region until it reaches a maximum local Mach number. Then, a shock is formed in the contour region. Similar as in the afterbody only, the shock location depends upon the contour surface and M_∞. The shock location for a given contour is more downstream for higher M_∞ and at the same M_∞, the shock location for SPS_1.1 is more downstream than SPS_1.2.

For the conical afterbody, the flow characteristic is the same as the other complete bodies up to the mid-section region. The expansion flow occurs at the turning angle, then the flow accelerated along the conical surface and weak shock is formed at the edge of base. Figure (8) shows the Mach number contour and corresponding residual calculation for conical afterbody at $M_\infty = 1.10$.

The pressure drag coefficient (C_d-press) versus free stream Mach number (M_∞) for fine grid complete bodies are plotted in figure (9). The drag rises sharply in the high subsonic Mach number ($M_\infty \approx 0.95$) and reaches a maximum (peak) at $M_\infty \approx 1.10$. Then the drag decreases with a shallow curve as the M_∞ increases. The decreasing shallow curve may be caused by the bluntness of the nose and it agrees with Shapiro[16] because the fineness ratio and bluntness of the nose of bodies of revolution are the important factors that contribute the drag curve at transonic and supersonic range. As can be seen from the graph, the drag curve for the complete body with a conical afterbody is higher than with the small perturbation solution contour for the entire M_∞-range. Furthermore, the peak of the drag curve is approximately 15% higher. The drag curve for SPS_1.1 and SPS_1.2 are likely to have the same trend up to $M_\infty = 0.95$; beyond this Mach number, the drag curve for SPS_1.2 is slightly greater than for SPS_1.1. Therefore, the complete body with small perturbation solution contour afterbody Mach 1.1 (SPS_1.1) relatively gives the lowest drag.

Conclusions and Recommendations

For any given body contour, the use of numerical simulation (CFD) appears to be the most cost effective method of predicting aerodynamic performance, especially in the transonic range. To be sure, the quality of the grid as well as the details of the turbulence formulation in the Navier-Stokes approach affect the validity of the results. In this research, the grid-generating program GRAPE was found suitable only for smoothly contoured surfaces (e.g., SPS_1.1 and SPS_1.2); the program GRIDGEN2D was used for the geometry of a conical afterbody because of its non-smooth points. We have also shown[2] that for a complete body model the use of a fine grid is required. This was evidenced by the absence of the bow shock at M_∞ > 1 for the coarser grids.

The pressure drag coefficient (C_d) versus free stream Mach number (M_∞) graphs show that the small perturbation solution contour for Mach 1.10 (SPS_1.1) gives relatively the lowest C_d on both models (after body and complete body), a decrease of nearly 15% in the transonic peak, compared to the conical afterbody. These results are true for both the viscous and inviscid calculations and, by the using the comparison with the same technique, we have shown a relative improvement. Therefore, an attractive design for axi-symmetric bodies such as missiles, projectiles and aircraft, can be based on the small perturbation solution contour studied.

References

1. Guderley, K. G., "The theory of Transonic Flow," Pergamon Press, London, 1962.

2. Liepmann, H. W., Roshko, A., "Elements of Gas Dynamics," John Wiley and Sons, Inc., 1957.

3. Nixon, D., "Transonic Aerodynamics," AIAA, Progress in Astronautics and Aeronautics, Vol. 81, 1982.

4. Sahu, J., "Numerical Computations of Transonic Critical Aerodynamic Behavior," AIAA Journal, Vol 28 No.5, May 1990.

5. Priyono, E., "An Investigation of the Transonic Pressure Drag Coefficient for Axisymmetric Bodies," MS Thesis, Naval Postgraduate School, 1994.

6. Biblarz, O., "Phase Plane Analysis of Transonic Flows," AIAA, Paper No. 76-332, July 1976.

7. Biblarz, O., "An Exact Solution to the Transonic Equation," Israel Journal of Technology, Vol. 13, 1975.

8. Al-hashel, W.I., "Two-Dimensional Boundary Surfaces for Axi-Symmetric External Transonic Flows," MS Thesis, Naval Postgraduate School, 1993.

9. Van Dyke, M.D., "Perturbation Methods in Fluid Mechanics," Academic Press, N.Y., 1964.

10. Chow, W.L., "Base Pressure of a Projectile Within the Transonic Flight Regime," AIAA Journal, Vol.23, No.3, March 1985.

11. Payne, P.R., "Drag of Conical and Circular Arc Afterbodies Without Jet Flow," Aviation and Surface Effect Department, Report DTNSRDC/ASED-80/10, May 1980.

12. Fletcher, C.A.J., "Computational Techniques for Fluid Dynamics," Vol I, Springer-Verlag, New York, 1990.

13. Sorenson, R.L., "A Computer Program to Generate Two-Dimensional Grids About Airfoils and Other Shapes by the Use of Poison's Equation," NASA Technical Memorandum 81198, 1981.

14. Steinbrenner,J.P., Chawner,J.R.,"The Gridgen V.8 Multiple Block Grid Generation Software," MDA Engineering, Inc., Arlington, Texas, December 1992.

15. Bunning, P.G., and others, "Overflow User's Manual Version 1.6g," NASA AMES Research Center, California, June, 1992.

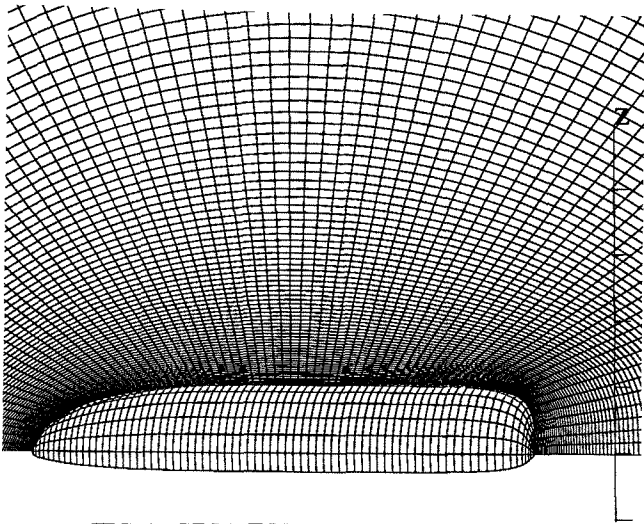16. Shapiro, A.H.,"The Dynamics and Thermodynamics of New York, 1954.
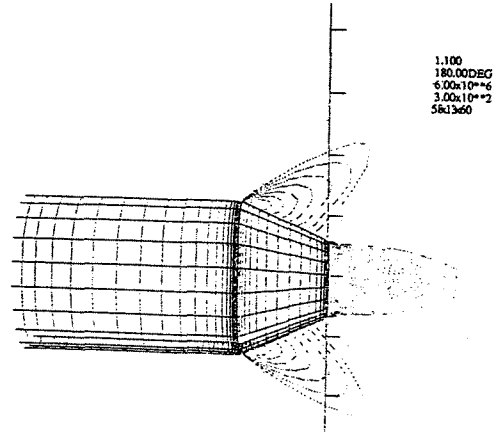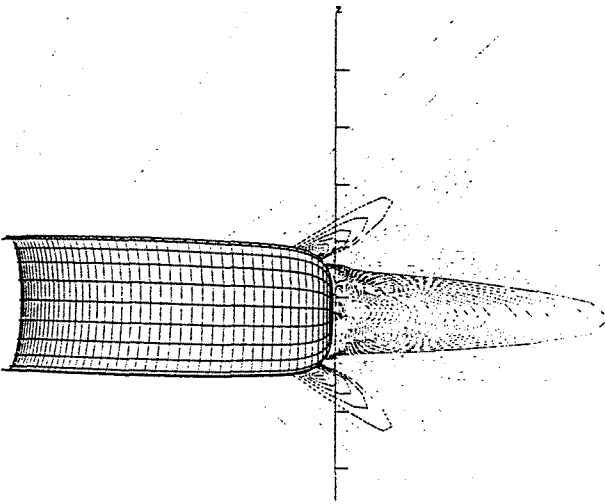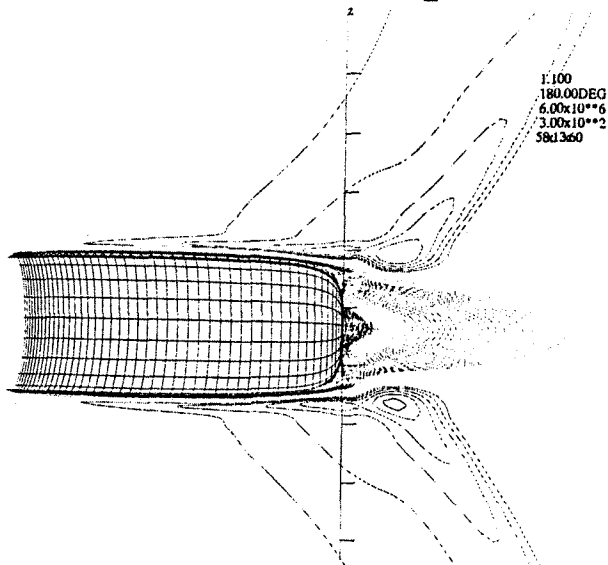
FIG 1. GRID FOR COMPLETE BODY

FIG 2. AFTERBODY MODEL SPS_1.1, INVISCID

FIG 3. AFTERBODY MODEL SPS_1.1, VISCOUS
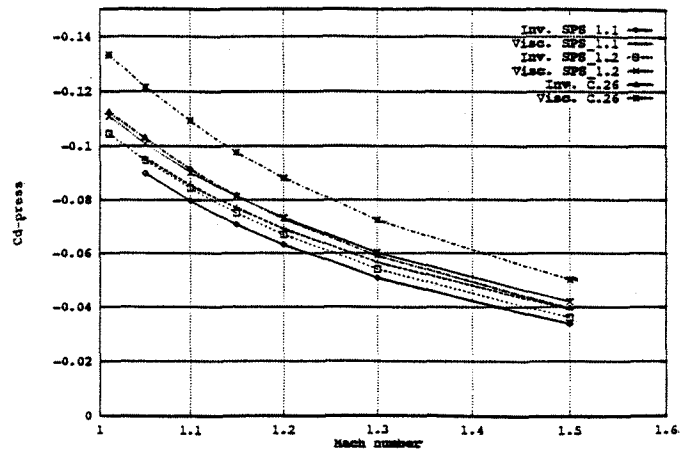

FIG 4. CONICAL MODEL, INVISCID
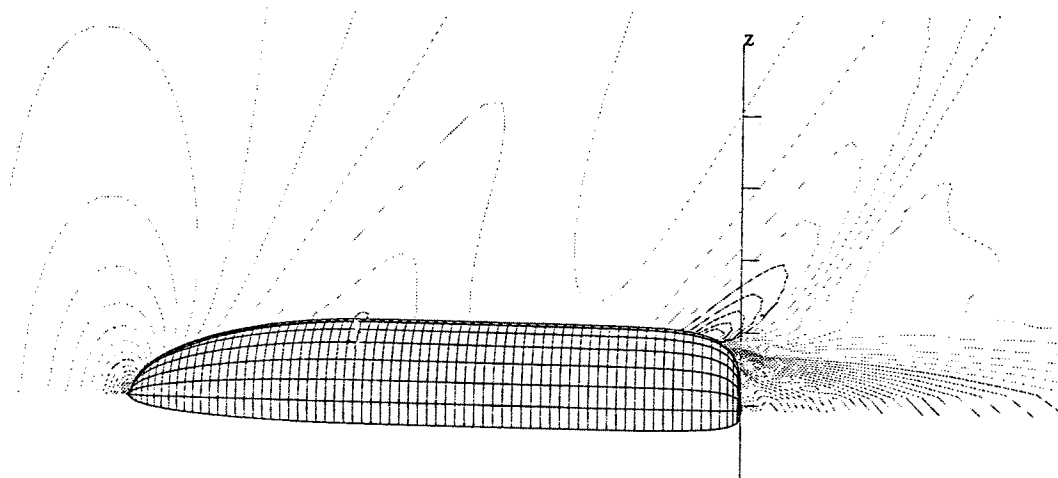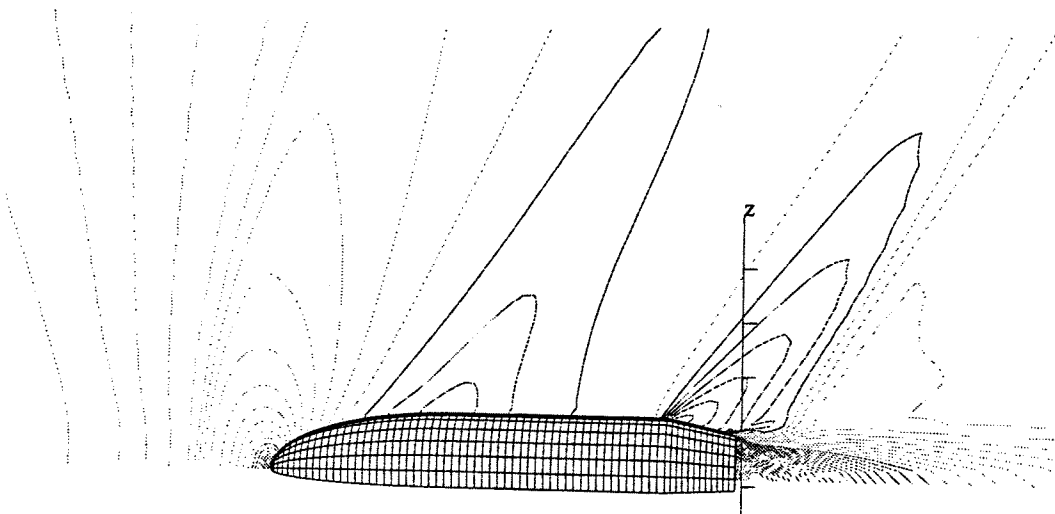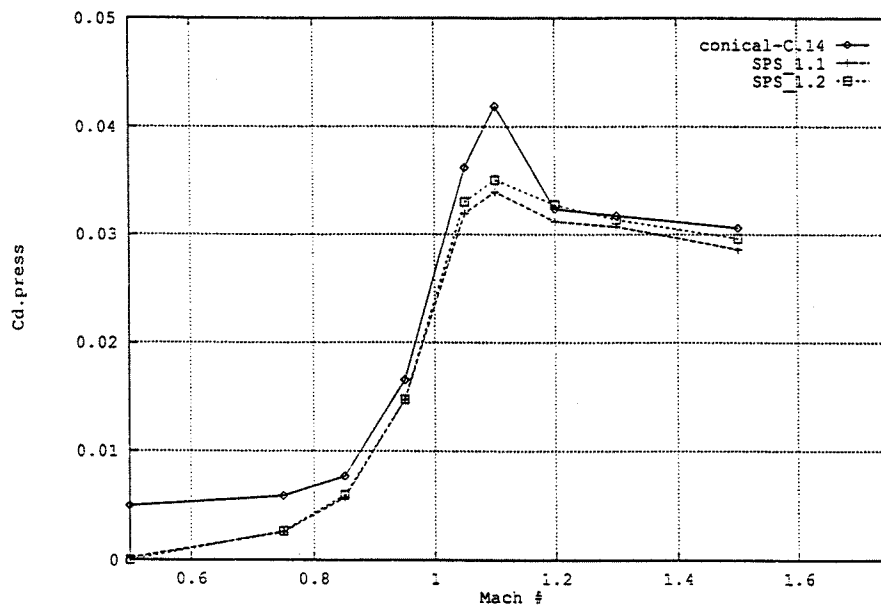

FIG 5. CONICAL MODEL, VISCOUS

FIG 6. C_d-PRESS VERSUS MACH NUMBER

COMPLETE BODY MACH CONTOUR SPS_1.2, INVISCID

COMPLETE BODY MACH CONTOUR CONICAL, INVISCID

C_d-PRESS VERSUS MACH NUMBER FOR COMPLETE BODY